PAPER

Redox cycling without reference electrodes†

Sahana Sarkar, Klaus Mathwig, Shuo Kang, Ab. F. Nieuwenhuis and Serge G. Lemay*

The reference electrode is a key component in electrochemical measurements, yet it remains a challenge to implement a reliable reference electrode in miniaturized electrochemical sensors. Here we explore experimentally and theoretically an alternative approach based on redox cycling which eliminates the reference electrode altogether. We show that shifts in the solution potential caused by the lack of reference can be understood quantitatively, and determine the requirements for accurate measurements in miniaturized systems in the absence of a reference electrode.

Introduction

Motivated by the wide applications of electrochemical sensors in the biomedical domain, there is continuously rising interest in miniaturised assays suitable for integration. Electrochemical sensors are particularly well suited for cost effective realization and integration with fluidics due to their inherent compatibility with microfabrication.[1–11] Irrespective of the particular measurement method employed (amperometry, potentiometry, impedance spectroscopy, *etc.*), the reference electrode is a key component of electrochemical sensors. In miniaturized systems, however, the volume-to-surface area ratio of reference electrodes decreases, thereby reducing their lifetime and stability.[12–16] For example, due to downscaling, dissolution of the electrode material, leakage of the reference solution and contamination at the junction of salt bridges become difficult to avoid, rendering many sensors short-lived or unreliable. Realizing lab-on-a-chip devices without the use of conventional reference electrodes[12,14–17] could therefore significantly improve the performance and usability of miniaturised electrochemical sensors.

One potential route for bypassing the reference electrode is offered by systems based on redox cycling, in which a current is generated by successively reducing and oxidizing an analyte at two independently biased electrodes. While the primary purpose of redox cycling is typically to increase the magnitude of the electrochemical current or to improve selectivity,[18–20] it also provides a pathway for electrochemically generated currents to flow through the analyte solution without the need for a reference or auxiliary electrode. In this work we explore the underlying principles of operation of redox cycling systems without a reference electrode. As a prototypical system we focus on fluidic nanogap sensors, shown in Fig. 1a, consisting of two closely spaced parallel electrodes separated by a few tens of nanometers and forming the floor and roof of a fluid-filled nanochannel. Electrochemically active molecules undergo successive redox cycling by diffusing back and forth between these electrodes, generating a current that is proportional to the analyte concentration. The cross-sectional diagram and top views of such a device are shown in Fig. 1b and c, respectively.
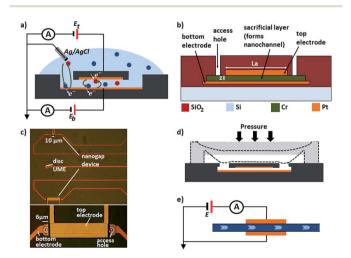

Fig. 1 (a) The nanogap sensor in the conventional 3-electrode configuration that includes a reference electrode. Redox molecules undergo successive oxidation and reduction reactions at the two planar electrodes while diffusing within the nanochannel. An ionic current also flows to the reference electrode. (b) The schematic diagram of the cross-section of the device prior to etching (not drawn to scale). La and z represent the active (or overlapping) length of the top and bottom electrodes and the height of the nanogap, respectively. (c) Optical microscopy image of the top view of the device before the sacrificial layer is etched. (d) The nanogap sensor with an integrated microfluidic valve (PDMS). In the closed state the reference electrode (not shown) gets disconnected, as represented by the dashed lines. (e) The capillary based fluid flow system consisting of two electrodes imbedded in a flow through the (nano) channel.

MESA + Institute for Nanotechnology, University of Twente, PO Box 217, 7500 AE Enschede, The Netherlands. E-mail: S.G.Lemay@utwente.nl; Fax: +31 53 489 3511; Tel: +31 53 489 2306

An example application of a variant of this device in which operation without a reference electrode would be necessary is a sealable chamber allowing locally generated analyte molecules (*e.g.*, by a catalytic reaction) to be collected and detected in a fL-level volume (Fig. 1d). Another example is the incorporation of a nanogap directly in (or, more practically, in a side channel of) a capillary flow detection system (Fig. 1e). Other configurations where the same general principles apply include interdigitated arrays[19,21–24] and ring-disk electrodes.[25,26]

We emphasize that this work does not in any way diminish the relevance of previous efforts at realizing miniaturized reference electrodes, but instead provides an alternative, complementary approach.

Materials and methods

A nanogap sensor with two parallel planar electrodes, as shown in Fig. 1a–c, was used in our experiments. The method for the micro-fabrication of the devices was similar to that reported previously.[27] In brief, the device consisted of a sacrificial chromium layer (thickness $z = 60 \pm 5$ nm) deposited between two platinum electrodes. The areas of the top and bottom electrodes were 60 μm^2 and 102 μm^2, respectively, whereas the overlapping area between the two electrodes where redox cycling took place was 30 μm^2. Prior to the measurements, a chromium etchant (BASF, Chromium Etch Selectipur) was filled through the inlets in order to etch the sacrificial layer and create the nanochannel. The electrodes were cleaned before conducting the measurements by cycling their potential in 5 mM H_2SO_4. A polydimethylsiloxane (PDMS) reservoir filled with analyte solution was positioned above the device and a standard Ag/AgCl electrode (BASi, MF 2079, RE-5B) inserted in this reservoir was used as the reference electrode. The reference electrode was thus located outside the nanochannel in the reservoir. No auxiliary electrode was necessary as the current through the reference electrode remained well below 1 nA, as shown in detail below (Fig. 2). All solutions were prepared in 18 MΩ cm Milli-Q water (Millipore). Ferrocenedimethanol ($Fc(MeOH)_2$, Sigma-Aldrich, cat. no-372625, diffusion coefficient $D = 6.7 \times 10^{-10}$ m^2 s^{-1}) was chosen as a simple prototypical redox species and was prepared as a 1 mM solution reduced $Fc(MeOH)_2$ with 0.1 M KCl (Sigma-Aldrich, cat. no-P3911) added as the supporting electrolyte.

In order to investigate the role of the reference electrode in redox cycling measurements, experiments were conducted with two complementary electrode configurations. In the first configuration the Ag/AgCl electrode was held at a fixed bias, thus serving as a suitable reference electrode, while the current flowing through it was monitored using a transimpedance amplifier (Femto, DDPCA-300). In the second scheme, there was no true reference electrode present. The standard Ag/AgCl reference electrode instead served as a non-invasive probe to the solution potential, E_{sol}. A Keithley 617 electrometer was used for these potentiometric measurements. The chassis ground and common (COM) terminals of all the instruments were connected together throughout the measurements; we refer to this potential as the circuit reference potential (or ground for short).
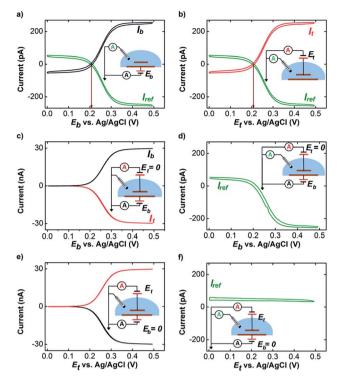

Fig. 2 Cyclic voltammograms for 1 mM Fc(MeOH)$_2$ in 0.1 M KCl at a scan rate of 5 mV s^{-1}. The black, red and green lines represent the currents measured at the top, bottom and reference electrodes, respectively. (a) The bottom electrode (E_b) was swept while the top electrode was left floating; the rest potential was $V_{rp} = 0.21$ V. (b) The top electrode (E_t) was swept while the bottom electrode was left floating; again $V_{rp} = 0.21$ V. (c) E_b was swept while E_t was biased at 0 V giving rise to a redox cycling current of 30 nA. (d) The current through the reference electrode during redox cycling, I_{ref}, was essentially identical to that observed in cases (a) and (b). (e) E_t was swept while E_b was biased at 0 V. (f) I_{ref} measured simultaneously with the voltammogram in panel (e). The current is nearly constant, in sharp contrast with panel (d).

Scan rates were kept sufficiently low such that steady-state mass transport conditions were achieved.

Experimental results

We first concentrate on measurements conducted with an active reference electrode. Fig. 2a shows the cyclic voltammogram obtained at the bottom electrode when its potential, E_b, was varied from 0 to 0.5 V while the potential of the top electrode, E_t, was disconnected (black curve). A sigmoidal cyclic voltammogram was observed with a wave height (the difference between the plateau currents at $E_t = 0$ V and $E_t = 0.5$ V) of $i_{lim} = 305$ pA. The cyclic voltammogram simultaneously obtained at the reference electrode is also shown (green curve); this current has the same magnitude but an opposite sign to that measured at the bottom electrode, demonstrating that all current from the working electrode flows to the reference electrode and therefore that there are no significant parasitic current leakage pathways in the system. The voltammogram (obtained at the bottom electrode) is shifted downward by 52 pA compared to that

expected for the original solution of $Fc(MeOH)_2$ in the reduced form. This indicates that this solution became partly oxidized after exposure to the reservoir, consistent with previous observations[28] and as verified explicitly by re-extracting the solution and analysing it *ex situ* (see ESI†).

Fig. 2b shows that sweeping E_t while keeping E_b floating gave rise to an essentially identical cyclic voltammogram. While this may appear counterintuitive since the top electrode is located further from the access holes, and thus one might expect smaller currents, this effect can be understood by noting that the bottom electrode must necessarily adjust its potential to that of the top electrode because of the strong coupling introduced by redox cycling, as discussed previously.[28] Similarly, measurements where both E_t and E_b were swept simultaneously (data not shown) yielded once again the same voltammogram. In all the above voltammograms, the potential at which the obtained current crosses the zero-current axis – that is, the rest potential, V_{rp} – was found to be 0.21 V.

Fig. 2c shows a typical voltammogram obtained during redox cycling with a reference electrode and E_b swept between 0 and 0.5 V while E_t was kept biased at 0 V. An oxidising current at the bottom electrode giving i_{lim} of 30 nA was observed. An equal and opposite current was observed at the top (reducing) electrode, as expected for redox cycling. The amplification factor for redox cycling can be defined as the ratio of i_{lim} at the electrode during redox cycling to that of the current at the reference electrode (Fig. 2a and c), yielding an amplification factor of ~98. It is however crucial to note that a finite current still flows through the reference electrode during redox cycling, as explicitly shown in Fig. 2d. This current originates from molecules from the bulk that diffused through the access holes into the channel, reacted at the bottom electrode and returned once again to the bulk reservoir. Correspondingly, the values of I_{ref} observed in Fig. 2d are essentially equal to those obtained in the case of Fig. 2a. Fig. 2e shows that when E_t was varied while E_b was biased at 0 V, oxidising and reducing currents were now observed at the top and bottom electrodes, respectively, as expected since the role of the electrodes was reversed. In this case, however, the current through the reference electrode (Fig. 2f) was roughly constant (apart from slight drift and hysteresis) with a value close to the $E_b = 0$ V values of 50 pA observed in Fig. 2a and c. This reflects the fact that mass transport to the reference electrode is much more efficient from the bottom than from the top electrode due to the channel geometry: the bottom electrode is directly exposed to the access holes, whereas molecules leaving the top electrode interact with near-certainty with the bottom electrode on their way to the bulk. As a result, the potential of the top electrode hardly influences I_{ref}.

We now turn to measurements done in the second configuration, in which no active reference electrode was used and the potential of the solution was allowed to float. Fig. 3a shows a cyclic voltammogram wherein E_t was biased at 0 V while E_b was cycled between −0.5 and 0.5 V with respect to the circuit reference potential. These curves are qualitatively different from those observed when the reference was connected (Fig. 2c), with both electrodes exhibiting reducing and oxidizing currents depending on the polarity of E_b. Thereafter, we introduced an
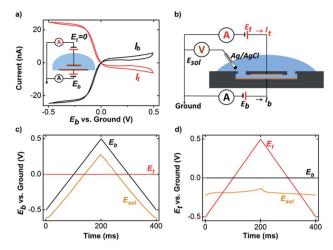

Fig. 3 Cyclic voltammograms for 1 mM $Fc(MeOH)_2$ in 0.1 M KCl at a scan rate of 5 mV s^{-1} in the absence of the reference electrode. (a) Currents obtained at the top (black) and bottom (red) electrodes when the bottom electrode (E_b) was swept while the top electrode (E_t) was biased at 0 V with respect to the circuit reference potential. (b) The schematic diagram of the setup configuration; the Ag/AgCl electrode now serves as a probe of the solution potential, E_{sol}. All potentials are referred to the external circuit potential, here labelled as Ground. (c) E_b was varied (black) while E_t was grounded (red) and E_{sol} was measured (orange). E_{sol} closely follows the potential of the sweeping electrode, E_b. (d) E_t was varied while E_b was grounded. E_{sol} experiences only minor variations compared to the sweeping potential, E_t.

Ag/AgCl electrode to monitor the potential of the floating bulk electrolyte with respect to the circuit reference potential, as shown in Fig. 3b.

Fig. 3c shows the corresponding measured potential of the solution, E_{sol} (orange curve) while cycling E_b (black curve) and keeping E_t equal to 0 V (red curve). E_{sol} follows the applied potential quite closely. Similarly, Fig. 3d shows the complementary case where E_t was cycled. In this case, sweeping the potential had a negligible effect on the bulk solution. These results illustrate qualitatively that the more effective mass transport from the bottom electrode to the bulk solution observed in Fig. 2 directly translates into a stronger influence of the bottom electrode on the solution potential.

Analysis

Using the measured potential of the solution, E_{sol}, and the known applied potentials, E_t and E_b (all referred to the external circuit potential), we can reconstruct the potential differences across the solid-liquid interfaces at both electrodes, $E_{t,sol}$ and $E_{b,sol}$. These are the preferred variables for describing electrochemical processes since it is these potential differences that drive electrochemical reactions. In terms of the directly measurable quantities defined above, these potentials are simply given by

$$E_{t/b,sol} = E_{t/b} - E_{sol} \qquad (1)$$

The potentials of Fig. 3c and d re-expressed in terms of $E_{t,sol}$ and $E_{b,sol}$ are shown in Fig. 4a and b, respectively. In Fig. 4a, it is
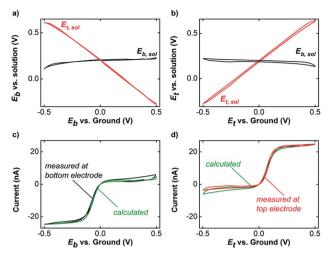
Fig. 4 (a) The potentials at the electrodes with respect to the solution, $E_{b,sol}$ and $E_{t,sol}$, while sweeping E_b. $E_{b,sol}$ remained relatively constant near a value of $V_{rp} = 0.21$ V while $E_{t,sol}$ varied from 0.6 V to -0.27 V. (b) The same as (a) except that E_t is swept. (c) The expected current was calculated using eqn (2) and the potentials of panel (a). The calculated and measured currents (represented as black and green lines, respectively) are in excellent agreement. (d) The same as (c) for the case where E_t is swept (panel b). The calculated and measured currents are represented as red and green lines, respectively.

observed that although E_b was swept over a broad range of potentials, $E_{b,sol}$ remained relatively constant near the V_{rp} at 0.21 V. In contrast, $E_{t,sol}$ changed from 0.6 V to -0.27 V, thereby showing that the top electrode was effectively being swept during the measurement while the bottom electrode held a nearly constant potential with respect to the solution. Fig. 4b shows exactly the same behaviour except that the potential curves are reflected through the $E_{t/b} = 0$ V axis. While this may appear to contrast with the large differences observed between Fig. 3c and d, this mirror symmetry must necessarily be present since, in the case where the solution potential is allowed to float, only the potential difference, $E_t - E_b$, can be relevant in establishing the interfacial potentials. Both electrode configurations thus lead to the same situation wherein the bottom electrode remains at a nearly constant potential while the top electrode experiences an effective potential sweep that is applied as a potential difference between the two electrodes.

In order to further test the validity of the values of $E_{t/b,sol}$ extracted above, we attempted to reconstitute the cyclic voltammograms of Fig. 3a using the potentials determined in Fig. 4a and b. The shape of redox-cycling voltammograms in nanogap devices has previously been shown to be well described by the Butler–Volmer formalism,[28]

$$I_t^{rc} = -I_b^{rc} = i_{lim} \frac{\dfrac{1}{1 + e^{-f\eta_t}} - \dfrac{1}{1 + e^{-f\eta_b}}}{1 + \dfrac{D}{k_0 z}\left(\dfrac{e^{\alpha f\eta_t}}{1 + e^{f\eta_t}} + \dfrac{e^{\alpha f\eta_b}}{1 + e^{f\eta_b}}\right)} \qquad (2)$$

Here z is the height of the nanochannel, $f = F/RT$, F is the Faraday constant, R is the gas constant, T is the absolute temperature and $\eta_{t,b}$ is the overpotential applied to the top and

bottom electrodes, respectively. That is, $\eta_{t/b} = E_{t/b,sol} - E_f$, where E_f is the formal potential of the reaction. E_f was measured directly using the same solution with a platinum UME (BASi, MF 2005) and the same reference electrode as used during the other measurements and was found to be 0.26 V. i_{lim} obtained during the redox cycling (30 nA, Fig. 2c and e) was directly substituted in eqn (2). The calculated value of i_{lim} is marginally higher ($\sim$32 nA) and this difference can be attributed to the buckling of the electrodes due to stress (resulting from the passivation) that leads to an increase in the height of the channel.[29] The remaining unknown parameters, *i.e.*, the transfer coefficient, α, and the heterogeneous rate constant, k_0, were found to be 0.50 and 0.06 m s^{-1}, respectively, consistent with previous measurements.[28]

Substituting the measured interfacial potentials from Fig. 4a and b into eqn (2) yields the calculated cyclic voltammograms (green curves) shown in Fig. 4c and d, respectively. These are in excellent agreement with the measured currents at the bottom (black curve) and top (red curve) electrodes obtained when E_b and E_t were swept, respectively.

Discussion

We first briefly summarize the situation for the classical system consisting of cyclic voltammetry at a UME. Within the operating window of the solvent, the detailed shape of the voltammogram depends on the solution composition and generically includes both a target analyte signal as well as parasitic currents resulting from reactions involving dissolved oxygen, hydronium ions and/or contaminants. Under typical steady-state mass transport conditions the current varies monotonically with electrode potential and vanishes at the rest potential, V_{rp}, as discussed before (Fig. 2a and b). A floating working electrode starting at an arbitrary potential will reduce or oxidize molecules in solution and accumulate charge until its potential drifts to V_{rp}, and this potential can be measured with a high-impedance voltmeter (Fig. 3). This description was further extended by Xiong and White to the case of a cell comprising of two polarisable electrodes in the absence of a reference electrode.[30]

The same principle applies to the redox-cycling case: in the absence of a reference electrode, the solution potential is determined by the condition such that no net current can be injected into the solution at a steady state,

$$I_t + I_b = 0 \qquad (3)$$

Here I_t and I_b are the currents at the top and bottom electrodes, respectively. That is, the solution potential will drift to the value at which eqn (3) is satisfied. In redox-cycling systems, the steady state current at each electrode can further be broken into two components: a redox-cycling current, $I_{t/b}^{rc}$, and an excess current, $I_{t/b}^0$. The latter includes all other current components such as parasitic reactions, irreversible reactions and reactions occurring in regions of the electrodes not implicated in redox cycling. This can be written as

$$I_{t/b} = I_{t/b}^0 + I_{t/b}^{rc} \qquad (4)$$

As can be seen in Fig. 2, the magnitude of $I_{t/b}^{rc}$ is far larger than $I_{t/b}^0$ and dominates the overall current levels during redox cycling. It is worth noting that the redox-cycling current obtained at the two electrodes is, by definition, equal and opposite ($I_t^{rc} = -I_b^{rc}$), however, eqn (1) and (2) reduce to the more specific condition

$$I_t^0 + I_b^0 = 0 \qquad (5)$$

That is, in the absence of a reference electrode, the potential of the electrolyte solution is fully determined by the excess current, $I_{t,b}^0$, even though it represents only a small fraction of the total currents flowing through the electrodes. This situation is reminiscent of positive-feedback scanning electrochemistry (SECM) measurements on a floating substrate,[31–36] but here it is the solution itself that adjusts its potential with respect to the electrodes.

Conclusions

Redox cycling measurements without a well-defined reference electrode are *a priori* difficult to interpret because it is not known how a potential difference applied between the two working electrodes is divided between them. We have argued that determining this potential is further complicated by the fact that it is fully determined by "excess" background currents rather than by the (usually much larger) redox cycling current. On the other hand, we have shown that the geometry of the redox cycling device can be exploited to alleviate this difficulty to a significant extent. In situations where one of the redox cycling electrodes has a much more significant exposure to the sample solution, this electrode can readily pin the solution potential to a nearly constant value, allowing the potential of the second electrode with respect to the solution to be controlled. While we have concentrated here on nanogap electrodes embedded in nanochannels, the same principles can be applied to other asymmetric redox cycling geometries such as recessed ring-disk electrodes or even interdigitated electrodes if one of the electrodes is recessed with respect to the other.

Acknowledgements

Notes and references

1 S. W. Dutse and N. A. Yusof, *Sensors*, 2011, **11**, 5754–5768.
2 T. M. H. Lee, M. C. Carles and I. M. Hsing, *Lab Chip*, 2003, **3**, 100–105.
3 T. A. Webster and E. D. Goluch, *Lab Chip*, 2012, **12**, 5195–5201.
4 A. Fragoso, D. Latta, N. Laboria, F. von Germar, T. E. Hansen-Hagge, W. Kemmner, C. Gartner, R. Klemm, K. S. Drese and C. K. O'Sullivan, *Lab Chip*, 2011, **11**, 625–631.
5 V. N. Goral, N. V. Zaytseva and A. J. Baeumner, *Lab Chip*, 2006, **6**, 414–421.
6 M. Koudelka-Hep and P. D. van der Wal, *Electrochim. Acta*, 2000, **45**, 2437–2441.
7 J. R. Kraly, R. E. Holcomb, Q. Guan and C. S. Henry, *Anal. Chim. Acta*, 2009, **653**, 23–35.
8 Y. H. Lin, D. W. Matson, W. D. Bennett, K. D. Thrall and C. Timchalk, *Microreact. Technol.: Ind. Prospects, Proc. Int. Conf., 3rd*, 2000, 588–596.
9 J. Wang, *Electroanalysis*, 2005, **17**, 1133–1140.
10 Z. W. Zou, J. H. Kai, M. J. Rust, J. Han and C. H. Ahn, *Sens. Actuators, A*, 2007, **136**, 518–526.
11 A. C. R. Grayson, R. S. Shawgo, Y. W. Li and M. J. Cima, *Adv. Drug Delivery Rev.*, 2004, **56**, 173–184.
12 M. W. Shinwari, D. Zhitomirsky, I. A. Deen, P. R. Selvaganapathy, M. J. Deen and D. Landheer, *Sensors*, 2010, **10**, 1679–1715.
13 H. Suzuki, *Electroanalysis*, 2000, **12**, 703–715.
14 M. A. Schwarz, B. Galliker, K. Fluri, T. Kappes and P. C. Hauser, *Analyst*, 2001, **126**, 147–151.
15 A. Simonis, H. Luth, J. Wang and M. J. Schoning, *Sens. Actuators, B*, 2004, **103**, 429–435.
16 R. K. Franklin, M. D. Johnson, K. A. Scott, J. H. Shim, H. Nam, D. R. Kipke and R. B. Brown, *IEEE Sens.*, 2005, 1400–1403.
17 H. Suzuki, H. Shiroishi, S. Sasaki and I. Karube, *Anal. Chem.*, 1999, **71**, 5069–5075.
18 B. Wolfrum, M. Zevenbergen and S. Lemay, *Anal. Chem.*, 2008, **80**, 972–977.
19 E. D. Goluch, B. Wolfrum, P. S. Singh, M. A. G. Zevenbergen and S. G. Lemay, *Anal. Bioanal. Chem.*, 2009, **394**, 447–456.
20 M. G. Straver, M. Odijk, W. Olthuis and A. van den Berg, *Lab Chip*, 2012, **12**, 1548–1553.
21 V. A. T. Dam, W. Olthuis and A. van den Berg, *Analyst*, 2007, **132**, 365–370.
22 J. I. Heo, D. S. Shim, G. T. Teixidor, S. Oh, M. J. Madou and H. Shin, *J. Electrochem. Soc.*, 2011, **158**, J76–J80.
23 O. Niwa, Y. Xu, H. B. Halsall and W. R. Heineman, *Anal. Chem.*, 1993, **65**, 1559–1563.
24 D. G. Sanderson and L. B. Anderson, *Anal. Chem.*, 1985, **57**, 2388–2393.
25 C. X. Ma, N. M. Contento, L. R. Gibson and P. W. Bohn, *ACS Nano*, 2013, **7**, 5483–5490.
26 G. Zhao, D. M. Giolando and J. R. Kirchhoff, *Anal. Chem.*, 1995, **67**, 1491–1495.
27 S. Kang, K. Mathwig and S. G. Lemay, *Lab Chip*, 2012, **12**, 1262–1267.
28 M. A. G. Zevenbergen, B. L. Wolfrum, E. D. Goluch, P. S. Singh and S. G. Lemay, *J. Am. Chem. Soc.*, 2009, **131**, 11471–11477.
29 M. A. G. Zevenbergen, D. Krapf, M. R. Zuiddam and S. G. Lemay, *Nano Lett.*, 2007, **7**, 384–388.

30 J. W. Xiong and H. S. White, *J. Electroanal. Chem.*, 2013, **688**, 354–359.

31 D. O. Wipf and A. J. Bard, *J. Electrochem. Soc.*, 1991, **138**, 469–474.

32 J. V. Macpherson, C. J. Slevin and P. R. Unwin, *J. Chem. Soc., Faraday Trans.*, 1996, **92**, 3799–3805.

33 Y. Selzer, I. Turyan and D. Mandler, *J. Phys. Chem. B*, 1999, **103**, 1509–1517.

34 C. G. Zoski, N. Simjee, O. Guenat and M. Koudelka-Hep, *Anal. Chem.*, 2004, **76**, 62–72.

35 H. Xiong, J. D. Guo and S. Amemiya, *Anal. Chem.*, 2007, **79**, 2735–2744.

36 A. I. Oleinick, D. Battistel, S. Daniele, I. Svir and C. Amatore, *Anal. Chem.*, 2011, **83**, 4887–4893.

Supporting Information

Redox Cycling Without Reference Electrode

Sahana Sarkar, Klaus Mathwig, Shuo Kang, Ab F. Nieuwenhuis and Serge. G. Lemay

1. Fabrication Methods

A nanogap sensor with two parallel planar electrodes, as sketched in Fig. 1a, was used for experiments. The method for microfabricating the devices is summarized here. The 20 nm thick platinum bottom electrode was deposited using electron beam evaporation using a Blazers BAK 600 system and patterned by photolithography and a lift off process using Arch Chemical OIR 907-17 as photoresist. A 60 ± 5 nm chromium sacrificial layer and a 100 nm platinum top electrode were subsequently deposited and patterned by the same procedure. The whole structure was buried in a passivation layer of 750 nm of silicon nitride using a Film PECVD Oxford 80 system. Using reactive ion etching (Etch RIE Plasma Therm 790), two access holes, 2 x 2 µm, were then etched through the passivation layer to allow the inflow of solution into the nanochannel. The top and cross sectional view of the device has been sketched as shown in Fig. S1.
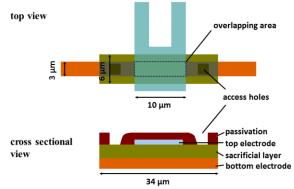

Figure S1: Top and cross sectional view of the device. The areas of the top and bottom electrodes are 60 µm^2 and 102 µm^2. The overlapping area is 30 µm^2 and represents the active area during redox cycling.

2. Characterization of solution after exposure to device

1 mM solution of Ferrocenedimethanol (Fc(MeOH)$_2$, Sigma-Aldrich, Catalog no. 372625, diffusion coefficient $D = 6.7 \times 10^{-10}$ m^2/s) nominally in the reduced form was prepared in Milli-Q water with 0.1 M KCl added as supporting electrolyte. Cyclic voltammetry was performed on this solution using a 10 µm diameter platinum ultramicroelectrode (BASi, MF-2005), as shown in Fig. S2 (blue curve). The sigmoidal oxidation wave confirmed that the Fc(MeOH)$_2$ was predominantly in the reduced form. A small amount of reducing current was also observed, presumably due to some contamination and consistent with other reports in the literature[1]. The crossing potential (V_{rp}) was found to be 0.17 V. A small volume of solution (ca. 80 µl) was then introduced in a Polydimethylsiloxane (PDMS) reservoir in contact with the device to perform measurements with the nanogap sensor. Prior to this, both the device and the reservoir had been exposed to a chromium etchant solution (BASF, Selectipur) which was used to etch the sacrificial layer of the nanochannel. Sulphuric acid had similarly been used to clean the electrodes. It is likely that residues from both the etchant and the acid were absorbed within the PDMS. After conducting the measurements with the nanogap device, the solution was extracted out

of the reservoir and cyclic voltammetry was performed again using the ultramicroelectrode, as shown in Fig. S2 (red curve). The voltammogram exhibits a much more pronounced reduction wave, leading to an increase in the value of the V_{rp} to 0.21 V. This indicates that the solution became oxidized when introduced in the reservoir due to contamination, consistent with the measurements performed with the nanogap device.
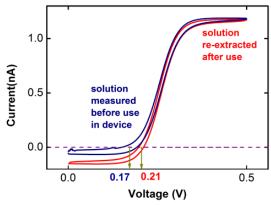

Figure S2: Cyclic voltammograms for 1mM Fc(MeOH)$_2$ in 0.1M KCl before (blue curve) and after (red curve) being introduced in the nanodevice (scan rate 10 mV/s).

1.   J. W. Xiong and H. S. White, *Journal of Electroanalytical Chemistry*, 2013, **688**, 354-359.